Desalination and Water Treatment
www.deswater.com
doi: 10.5004/dwt.2020.25814

194 (2020) 19–36
August

Experimental investigation of impact of ion and erosion on corrosion characteristics of aluminum alloy tubes in thermal desalination project

Xingsen Mu[a,*], Qimei Zheng[a], Wenjie Zhang[a], Ramuel Safakoolan[b], Gangtao Liang[a], Shengqiang Shen[a,*]

[a]*School of Energy and Power Engineering, Dalian University of Technology, Dalian, Liaoning Province, China, email: muxingsen@dlut.edu.cn (X. Mu), 1518325338@qq.com (Q. Zheng), 814816319@qq.com (W. Zhang), gtliang@dlut.edu.cn (G. Liang), zzbshen@dlut.edu.cn (S. Shen)*
[b]*Mechanical and Aerospace Engineering, University of California-Davis, Davis, California, USA, email: rsafarkoolan@ucdavis.edu (R. Safakoolan)*

Received 15 September 2019; Accepted 7 March 2020

ABSTRACT

3FL aluminum alloy is a recent advancement in 5xxx series alloys which is developed to prevent Cl^+ corrosion. The possibility of a 3FL aluminum alloy applied to desalination is discussed in this paper. The corrosion of the material of the test tube is quantitatively analyzed by the electrochemical corrosion experiment. The corrosion changes of the test tubes after seawater treatment under different operational conditions are analyzed by horizontal tubes falling film evaporation corrosion experiments. The results show the concentration of Cu^{2+} and Fe^{3+} in the experiment without ion trap is about seven times that in the experiment with an ion trap. With the concentration decrease of Fe^{3+} and Cu^{2+}, the average density, depth, and diameter of pitting corrosion are significantly reduced. By increasing the tube pitch, the deposition of $CaCO_3$ on the surface of the tube is reduced. Seawater scour increases the diameter of pitting corrosion and pitting density. As deionization time increases, the corrosion current density and corrosion rate decrease obviously. Therefore, deoxidization, ion trap, and decline of tube pitch must be considered in the design of the evaporator. It is recommended to use a rotated triangular tube layout or quadrilateral tube arrangement.

Keywords: Seawater desalination; 3FL aluminum alloy tubes; Corrosion morphology; Pitting corrosion

1. Introduction

The shortage of freshwater in the world has led to the rapid development of desalination technology, and low temperature-multi effect distillation (LT-MED) technology is one of the crucial technologies in thermal desalination technology [1]. Most of the heat transfer tubes used throughout this technology in engineering are aluminum brass tubes and titanium alloy tubes. As the price increase of copper and titanium in recent years, the advantages of using aluminum alloy tubes appeared, which in the character of low price, good thermal conductivity, and good corrosion resistance under natural conditions [2].

The following is a brief summary of the related researches on the corrosion characteristics of aluminum alloys. (1) The major studying points on the aluminum alloy itself are various components [3] processing technology [4–6], and the state of the material surface [7], etc. Guo-jun and Xin-yu [3] analyzed 7055 aluminum alloys which have the highest strength among the strongest deformed aluminum alloys by conductivity curve and age hardening curve, concluded the higher electrical conductivity, the better resistance to stress corrosion. (2) The major studying points on the state of the corrosive medium are about dissolved oxygen concentration [8–10], salinity [11], flow rate [12,13], temperature [14,15], pH [16,17], and heavy metal ion concentration [18,19], etc. Ahmed [9] studied the effect of DO concentration on the

* Corresponding authors.

pitting corrosion of aluminum alloy tubes by experiment. The results show that the DO concentration of seawater is needed to reduce to less than 30 ppb when the pH of seawater is between 7.5 and 8.2. Wencai et al. [10] studied the influence of temperature and dissolved oxygen on the electrochemical performance of 5083 aluminum alloy in seawater corrosion. It is obtained that as the DO concentration decreases, the self-corrosion potential of aluminum alloy moves negatively and the pitting potential of aluminum alloy shifts negatively with increasing temperature. Yu-zhou et al. [20] emphasized that high-speed seawater will cause abrasion corrosion, impact corrosion, and cavitation corrosion, which will aggravate the corrosion of aluminum alloy. The velocity of seawater in the deep ocean is slower than that of the surface layer, the corrosion rate of aluminum alloy will decrease accordingly.

Up to now, there are numerous researches on different types of aluminum alloys under a single specific operational condition. Zhiguo [21] researched the characteristic of 5052 aluminum alloy in seawater which removes the copper and iron ions (Cu^{2+} and Fe^{3+}) by redox reaction using reductant. The results show that when the concentration of the two metal ions is 50 ppm, the average corrosion rate of the aluminum alloy is four times that without adding the two metal ions. Abiola and Otaigbe [22] measured the corrosion rate of 2S aluminum alloy in four different aqueous solutions through weight loss experiments. As a result, the corrosion rates in the four solutions were [Cl^-, Fe^{3+}, Cu^{2+}] > [Cl^-, Cu^{2+}] > [Cl^-, Fe^{3+}] > [Fe^{3+}, Cu^{2+}]. This points out that Cl^- destroyed the metal surface oxide film in this process, and provided conditions for the reaction between heavy metal ions and the aluminum matrix. Scholars [23,24] studied corrosion of 5083 aluminum alloys in seawater through corrosion electrochemical experiments. It was found that when the concentration of active chlorine in still seawater is lower than 1 mg/L, its oxidation is beneficial to the passivation and improved pitting resistance. Bazzi et al. [25] used electrochemical experiments to study the corrosion characteristics of 3003 and 6063 aluminum alloys in a 3% NaCl solution at different temperatures.

From the above, we can discover that most scholars research on 5052, 2S, 5083, 3003, and 6063 of aluminum alloys, but less on 3FL aluminum alloys. Most researchers focus on the corrosion of different aluminum alloys in a single environment or specific ions and more emphasized on corrosion mechanisms. For engineering, especially under the special conditions that the seawater is saturated, the pressure is negative pressure, the surface of the heat transfer tube is washed with spraying seawater and the dissolved oxygen concentration is low, has not been fully studied and the design ideas of how to use aluminum alloy tubes to avoid corrosion in evaporator design are rarely mentioned. The relevant experiments and theoretical analysis are carried out to address the above issues in this paper. The electrochemical corrosion performance of 3FL aluminum alloy is analyzed by electrochemical experiments. The effects of deoxidation, Cu^{2+} and Fe^{3+} concentrations, and seawater scour on the corrosion characteristics of aluminum alloy tube surfaces are analyzed in detail, and put forward the design factors and design ideas when the aluminum tube is used in LT-MED evaporator.

2. Experimental method

This paper contains two kinds of experiments, the first one is the corrosion electrochemical experiment, and the second one is the horizontal tubes falling film evaporation corrosion experiment. The corrosion electrochemical experiment mainly analyzes the corrosion resistance of 3FL aluminum alloy tubes in seawater under different conditions, to take matching measures to suppress the corrosion of heat transfer tubes. The horizontal tubes falling film evaporation corrosion experiment mainly investigates the effects of dissolved oxygen concentration, concentrations of Cu^{2+} and Fe^{3+} in seawater and the seawater erosion on the corrosion characteristics of 3FL aluminum alloy tube surfaces, especially pitting corrosion. This is more targeted for the research on the measures to inhibit the corrosion of aluminum alloy heat transfer tubes.

2.1. Corrosion electrochemical experiment

2.1.1. Experimental pretreatment process

The experimental pretreatment process is mainly divided into two parts: the first part is the electrode pretreatment stage.

Cutting a 20 mm × 10 mm sample on the surface of the aluminum alloy by wire cutting. Sanding the curved surface into a flat surface, and then using a hand drill to open a 2 mm through a hole at one end of the sample. Connecting the wire to the sample with a screw. Then polishing the sample step by step until the roughness of the surface reaches Ra = 0.1. The surface of the sample is rinsed with deionized water, and the surface is dehydrated and decontaminated with absolute ethanol. Then putting the sample in a stoving chest to dry and intercepting a work surface area of 10 mm × 10 mm, the remaining area is sealed with epoxy resin. After the epoxy resin is completely cured, the polishing surface of the aluminum alloy electrode is polished with a polishing machine, then connecting the electrochemical workstation to do an electrochemical test.

The second part is the seawater pretreatment stage. Mainly dividing into two parts, one is to use the ion trap to perform deionization treatment on seawater at for 0, 10, 20, 50, and 90 min. Then taking seawater under different operational conditions to measure the concentration of Cu^{2+} and Fe^{3+} by the plasma emission spectrometer, which is shown in Table 1 below. The second is to use high-purity nitrogen to deoxidize the experimental seawater for 10 and 30 min, using the rubber to seal test device after

Table 1
Concentration of Cu^{2+} and Fe^{3+} in the samples

Sampling time (min)	Cu^{2+}concentration (ppb)	Fe^{3+}concentration (ppb)
0	22.4	12.7
10	13.4	5.9
20	7.3	3.8
50	5.2	2.0
90	2.9	1.7

deoxidation to avoid the dissolution of external oxygen. The dissolved oxygen concentration in seawater after deoxidation is 1.07 and 0.26 ppm.

2.1.2. Corrosion electrochemical experimental procedure

After pretreatment, connecting the experimental equipments as shown in Fig. 1.

Nitrogen is passed into an electrochemical cell placed in a water bath at a constant temperature of 24°C. A three-electrode system (saturated calomel electrode, the working electrode, and auxiliary electrode) and a salt bridge (a high-concentration electrolyte solution connecting the two solutions to lessen the liquid junction potential) are inserted into the solution. The electrode is connected to an electrochemical workstation to process the generated signals of voltage and current. Then connect to a computer for data processing by the Tafel curve extrapolation method to get the Tafel polarization curve.

The working electrode of the aluminum alloy is gradually passivated in the aqueous solution during the experiment. It needs time to stabilize because the potential of the working electrode will constantly move positively. When the stability time is 30 min, the amplitude of the potential change is already small, which is called the open circuit potential (OCP). The set potential range is –0.3~+0.3 V. The scanning direction is from cathode to anode. The scanning speed is 0.001 V and the scanning accuracy is set to $10e^{-5}$ adaptive precision. The main equipment parameters in the experiment are shown in Table 2.

2.2. Horizontal tubes falling film evaporation corrosion experiment

2.2.1. Materials and seawater in corrosion experiments

Test tubes made of 3FL aluminum alloy are a recent advancement in 5xxx series alloys which are developed to prevent Cl^- corrosion. 3FL aluminum alloy consisting mainly of metallic element such as Al and Mg exhibits good pitting corrosion resistance. The material composition of the 3FL aluminum alloy is given in Table 3.

The seawater used in the experiments has been taken from the Yellow Sea nearby Dalian of China. Properties of the seawater are given in Table 4. The concentration of Mg^{2+} is higher than that of other seawaters, perhaps due to the abundant magnesium resources in Dalian coastal.

2.2.2. Experimental apparatus in corrosion experiments

The main purpose of this experiment is to test the corrosion properties of 3FL heat transfer tubes in the LT-MED evaporator. As shown in Fig. 2, the experimental apparatus contains an ion trap pretreatment system, a deaerator system, a corrosion testing system, a steam condensing system, and a data acquisition system. Seawater is heated to a needed temperature in a water tank with electric power. The experimental seawater circulates in the ion trap pretreatment system. After a while, the concentration of Cu^{2+} and Fe^{3+} decrease to needed concentration (3 ppb in this paper). At the same time, according to Henry's law [26], the pressure of the corrosion system and the deaerator are maintained at saturation pressure to remove oxygen deeply. The DO concentration of seawater is kept at 120 ppb. After that, the pretreated seawater circulates in the corrosion system for 150 h. An observation window is installed on the evaporator, which is used to observe the surface macroscopic morphology changes on the test tube. The test tank is a sampler that is used to collect the seawater from the outlets of the deaerator and evaporator. A DO meter installed in the test tank is used to measure the concentration of DO. The water pump is used to circulate the experimental seawater. The steam is condensed to freshwater in the condenser. The freshwater flows into the water tank through pipelines. The non-condensable gases are discharged by a vacuum pump

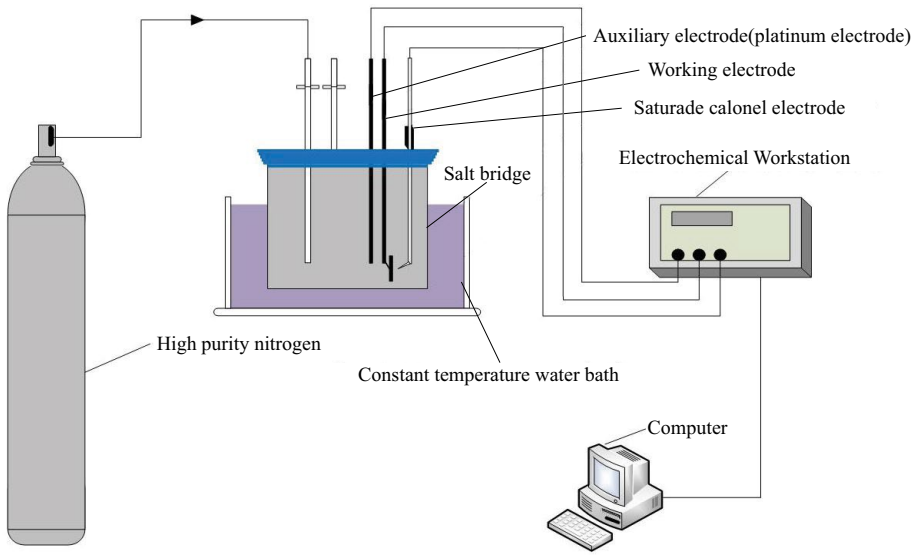

Fig. 1. Experimental apparatus of corrosion electrochemistry.

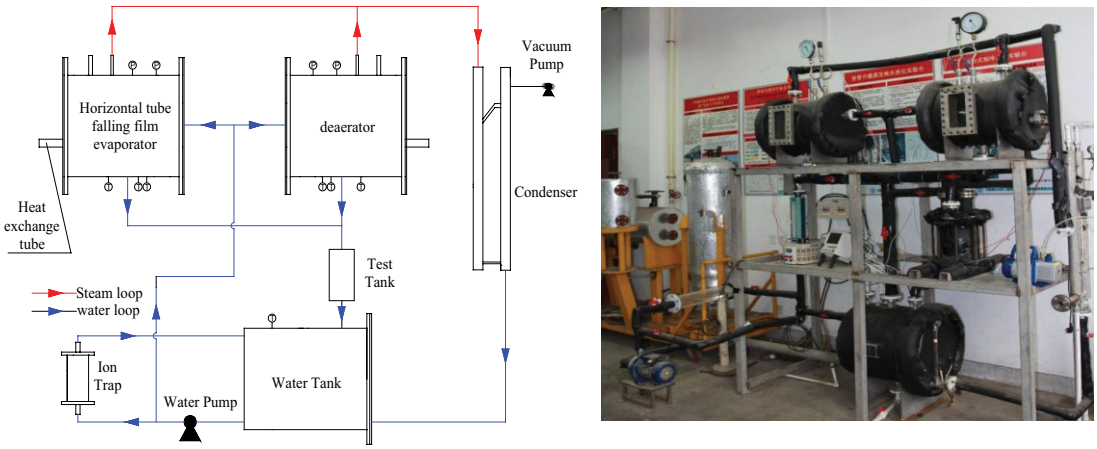

Fig. 2. Schematic of the experimental apparatus and experimental apparatus.

Table 2
Main experimental equipment

Name	Type	Measurement and accuracy
Plasma emission spectrometer	Optima 2000DV	Wavelength: 190–800 nm Elemental concentration: 1 ppb-1%
Electric thermostatic water bath	DK-S14	Temperature: 5°C–30°C Temperature precision: ±0.1°C
Polisher	3M7403	No load velocity: 3,000 rpm PSI: 57–95
Electrochemical workstation	CS300	Potential measurement: 0–±2.5 V Potential precision: 1 mV Current measurement:0–±2 A Current precision: 1 nA

Table 3
Mass percent composition of 3FL sample used in corrosion experiments

Alloy	Composition (mass %)							
	Iron (Fe)	Silion (Si)	Copper (Cu)	Magnesium (Mg)	Manganese (Mn)	Zinc (Zn)	Titanium (Ti)	Aluminum (Al)
3FL	≤0.15	≤0.13	≤0.005	0.40–1.80	≤0.10	≤0.005	0.01–0.03	Balance

through the condenser. To reduce the heat loss, thermal insulation is attached to the evaporator body, the deaerator body, and the circulation loop.

The structure of the horizontal tubes falling film evaporator is shown in Fig. 3. The pretreated seawater sprays to the dummy tube and then sprays to the test tube evenly. The dummy tube and the test tube are both made of the 3FL aluminum alloy tubes, with the outer diameter of 25.4 mm and the thickness of 1.65 mm. The effective length of test tubes with an electric heater inside is 330 mm. All the temperature measurements are made with thermocouples calibrated to an accuracy of 0.1°C. The pressure of the experimental system is measured by pressure transducers and precision pressure gauges. The accuracy of the pressure transducers is 0.4 grade. During the experiment, the data is collected by a model HFM-215 data acquisition meter.

All the measuring instruments used in this experiment are produced by regular manufacturers on the market and had been calibrated many times to ensure accuracy. Among them, the calibration results of thermocouples and pressure sensors indicate that they have good linearity. Besides, the dissolved oxygen meter of Pro ODO used directly in vacuum has less accurate. So, the dissolved oxygen meter of Pro ODO uses the dissolved oxygen meter of OXY2401 which has higher accuracy than Pro ODO cannot be used directly under vacuum, for multiple calibrations to ensure the accuracy of the measured values. The types, accuracy and range of the instruments used in the experiment are shown in Table 5.

With n direct measurement parameters X_1, X_2,…,X_j…, X_n, for each measurement n times, the best estimate is obtained.

$$\bar{x} = \frac{1}{N}\sum_{j=1}^{n} x_j \tag{1}$$

The standard deviation (uncertainty) is:

$$\sigma_x = \sqrt{\frac{1}{N-1}\sum_{j=1}^{n}\left(\bar{x} - x_j\right)^2} \tag{2}$$

Table 4
Parameters of seawater used in the corrosion test (the unit of the concentration is mg/L in the table)

Parameters	Value
pH	7.89
Sulfur (S)	2.9%
Calcium ion (Ca^{2+})	247.4
Magnesium (Mg^{2+})	3,460
Copper ion (Cu^{2+})	0.0224
Iron ion (Fe^{3+})	0.0128

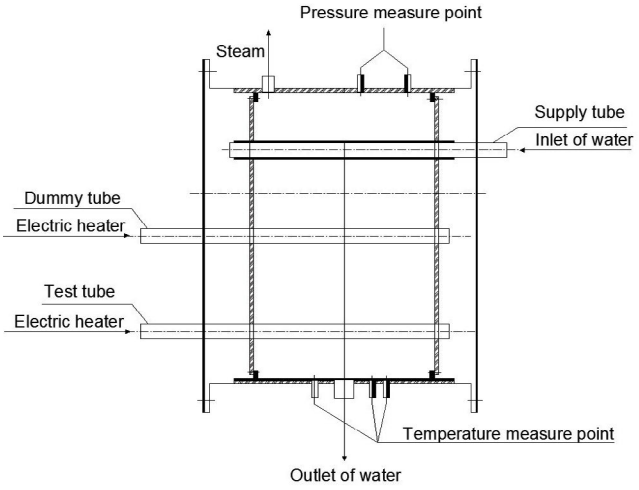

Fig. 3. Structure of the horizontal tubes falling film evaporator.

If there are indirect measurement parameters,

$$y = f\left(x_1, x_2, \cdots, x_n\right) \tag{3}$$

then the standard deviation of error transfer rule is as follows.

$$\sigma_y = \sqrt{\sum_{j=1}^{n}\left(\frac{\partial y}{\partial x}\sigma_x\right)^2} \tag{4}$$

The relative error is usually used in the actual calculation.

The main parameters involved in this experiment are the concentration of Cu^{2+} and Fe^{3+}, oxygen concentration, and pH value. The concentrations of heavy metal ions are measured by a spectrometer measuring the number of photons falling on the pixel. The oxygen concentration is obtained by a series of conversions of the primary battery current detected by the secondary ammeter. Ultimately, the uncertainty of each measurement is calculated by referring to the parameters of the relevant instruments and the accuracy of the direct measurement, as shown in Table 6.

The deionization process took place in the ion trap (Fig. 4) with a length of 500 mm, an inner diameter of 100 mm and an effective volume of 3.925 L. The main body of the ion trap is made of organic glass and the ion trap is filled with 3FL aluminum alloy rings with a packed density of 88.74%. The volume of the experimental seawater is 75 L.

2.2.3. Experiment conditions and experiment process in corrosion experiments

The experimental conditions are similar to the actual operational conditions of the LT-MED desalination system. In the experiment, the basic condition is that the seawater temperature is 60°C, the salinity is 2.9%, the system pressure is 19.9 kPa, the spray density of the seawater in the evaporator is 0.1 kg/(m s), and the DO concentration in the experimental seawater maintains at 120 ppb.

There are three main types of operational conditions in this paper, as shown in Table 7.

The first operational condition is deoxidation with the dummy tube. The DO concentration of seawater is 120 ppb. The second operational condition is deoxidation and deionization with the dummy tube. After treatment, the

Table 5
Error of the meters used in the experiment

Meter	Equipment model	Range	Accuracy
DO meter	Pro ODO	0–50 mg/L	±10 ppb
DO meter	OXY2401	0–50 mg/L	±1 ppb
pH meter	Five Go	0–14	0.01
ICP	PerkinElmer ICP8000	Ultramicro to constant	1 ppb
Thermocouple	T type	–200°C–400°C	0.1°C
Pressure transducer	YB150	0–200 MPa	0.4 Grade
Pressure gauge	UNIK PMP5073	0–100 kPa	±1%
Salinity meter	Testo 240	1 mg/L–200 g/L	1 mg/L

Table 6
Uncertainty of related parameters

Parameter	Measuring range	Uncertain
The concentration of Fe^{3+}	0.0020–0.0230	±1%
The concentration of Cu^{2+}	0.0010–0.0200	±1%
Dissolved oxygen concentration	0.20–7.30	±2%
PH value	7.50–8.50	±2%

concentration of heavy metal ions in the experimental seawater is less than 5 ppb, and the DO concentration is 120 ppb. The third operational condition is to remove the aluminum alloy dummy tube between the test tube and the supply tube, which is based on the second operational condition to study the influence of seawater scouring on the corrosion of the test tubes.

The specific steps of the experiment are as follows. Different pretreated seawater is selected as the corrosive medium, and the experimental tube section is selected from the 3FL aluminum alloy tube with the outer diameter of 25.4 mm. The salinity of the experimental seawater is 2.9%, and the experimental time of each experiment is 150 h. First, turn on the deionization system for deionization and complete seawater sampling. After turning off the deionization system, turn on the deoxidation system and adjust the heater power to maintain the seawater at 60°C. Then turn on the vacuum pump and dissolved oxygen meter to maintain the experimental system at 20 kPa, and when the dissolved oxygen concentration drops to 120 ppb, turn off the heating device of the oxygen removal system. Second, open the water inlet valve and drain valve of the corrosion test system. After 10 min, the water inlet valves of the deaerator are closed. When the spray condition of the evaporator is stable, the heating device in the experimental tube is turned on until the power is stabilized at 350 W. The corrosion test is performed for 10 h every day. Finally, after the experiment, turn off all heating devices and turn off the water pump to stop the circulating water flow after 15 min. Use high purified nitrogen to raise the system pressure to 50 kPa, and close all the valves of the evaporator and deaerator. Continue to pass high purified nitrogen to raise the pressure in the water tank to 75 kPa, and take a sample through the water intake valve in the ion trap system for subsequent metal ion concentration testing. After the 150 h corrosion test is completed, the test tube is removed for subsequent testing and analysis.

During the experiment, the surfaces of the test tubes are observed and photographed through the observation window (photographing frequency is 3 time/h) and the DO concentration in seawater is monitored in real-time. The morphology changes of the surfaces of the test tubes are recorded for the law of the generation and development of pitting corrosion. After the end of the 150 h corrosion experiment, the test tubes are taken out from the evaporator, and the macroscopic morphology of the surfaces of the test tube are observed and photographed. The test tubes are intercepted to several sections, and parts of the test tubes are rinsed with clean water, and then place in a stoving chest to dry. These are mainly used to analyze the surface corrosion morphology and corrosion product composition of the test tubes. The other parts should be corroded as the corrosion sample by the Chinese national standard which is to remove the surfaces of the test tubes by concentrated nitric acid and to rinse with deionized water. These are mainly used to analyze the pitting characteristics of the surface of the test tubes. Throughout the experiment, the tube surface morphology is observed with the scanning electron microscopy (SEM) (SUPARR 55). The corrosion product on the tube surface is analyzed by the energy disperse

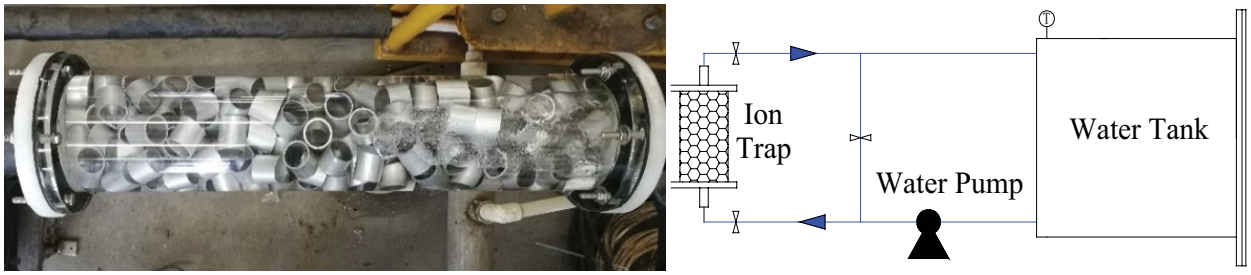

Fig. 4. Picture and structure of ion trap.

Table 7
List of experimental conditions

Number of operational condition	Name of operational condition	Corresponding picture
1	Deoxidation with dummy tube (DO:120 ppb)	Fig. 9
2	Deoxidation and deionization with dummy tube (DO:120 ppb, heavy metal ions < 5 ppb)	Figs. 9 and 17
3	Deoxidation and deionization without dummy tube (DO:120 ppb, heavy metal ions < 5 ppb)	Fig. 17

spectroscopy (EDS). The concentration of Cu^{2+} and Fe^{3+} in the experimental seawater is tested by the inductively coupled plasma (ICP) (Optima 8000).

3. Results and discussions

There are three operational conditions in this paper from Table 6 and the non-deoxidation experimental conditions are not involved. In the previous experiment, it is found that after 120 h of the experiment, a significant amount of corrosion is observed by the naked eye, and the non-deoxidation experiment has been carried out in detail [27] shown in Fig. 5 below.

No deoxidation condition is carried out for 150 h and when the experiment is carried out for 120 h, the severe corrosion on the surface of the test tube can be observed. So the experiment in this paper will not discuss the non-deoxidation conditions.

In this paper, the relevant electrochemical analysis of the deoxidation condition is as follows: oxygen acts as a depolarizer for the corrosion reaction, and changes of oxygen concentration have a direct effect on the rate of corrosion reaction. The polarization curves of the working electrode in seawater with different oxygen concentrations are tested by using an electrochemical workstation shown in Fig. 6. The corrosion current density is obtained by using the fitting software (chi750e) of workstation, and the corrosion rate is calculated by Eq. (5) [28].

$$C_R = 3.27\times10^{-3}\times\frac{MI_{corr}}{n\rho}\left(\text{mm/a}\right) \tag{5}$$

where M is the relative atomic weight of the metal; I_{corr} is the corrosion current density, mA/m^2, n is the number of lost electrons in the reaction formula, n = 3; ρ is the density of metal, ρ = 2.7 g/cm^3.

The experimental data in Table 8 shows that as the oxygen concentration decreases in seawater, the OCP gradually shifts negatively. With the decreases of oxygen concentration, the passivation degree of the surface of the working electrode weakens, and the OCP continuously moves negatively, as a result of the corrosion current density and corrosion rate decrease significantly. When the oxygen concentration is lowered from 7.29 to 1.07 ppm, the corrosion current density decreases by 43.7%. When the oxygen concentration is further lowered to 0.26 ppm, the corrosion current density at this time is reduced by 54.5% compared to the undeoxidized seawater. The corrosion rate has the same change law. Therefore, the deoxidation treatment of seawater is an important pretreatment step to reduce the corrosion rate of materials and inhibit the oxygen absorption corrosion of 3FL aluminum alloy.

3.1. Analysis of deioning process

The deion process is finished before the corrosion experiment. The total length of the deionization process is 90 min, and the frequency of sampling is one sample every 5 min. The concentration changes of Cu^{2+} and Fe^{3+} are shown in Fig. 7, while the temperature of seawater is 60°C in the ion trap. The reactions in the ion trap are listed as Eqs. (6) and (7).

The anode reaction:

$$Al - 3e^- \rightarrow Al^{3+} \tag{6}$$

The cathode reaction:

$$Fe^{3+} + 3e^- \rightarrow Fe; \quad Cu^{2+} + 2e^- \rightarrow Cu \tag{7}$$

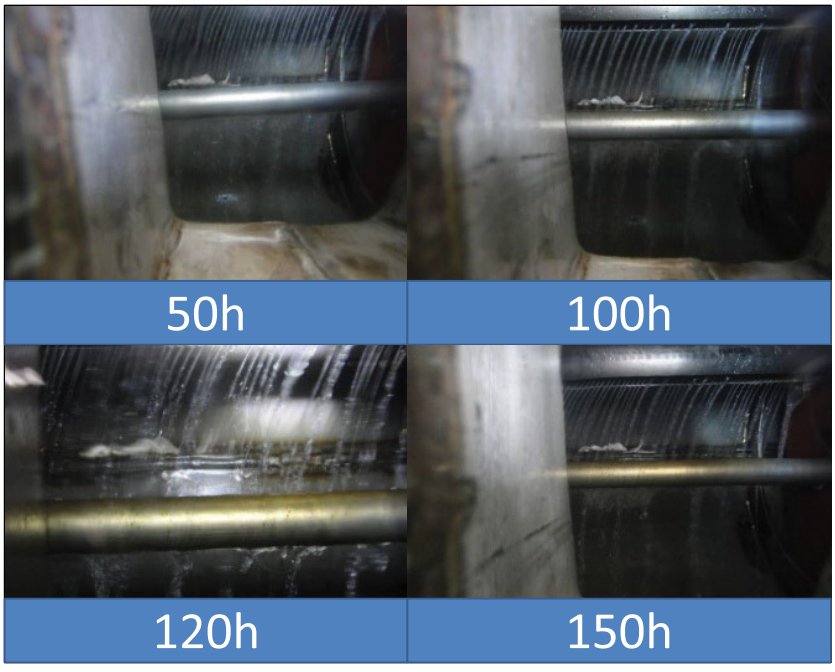

Fig. 5. Corrosion tube surface at different time periods without deoxidation.

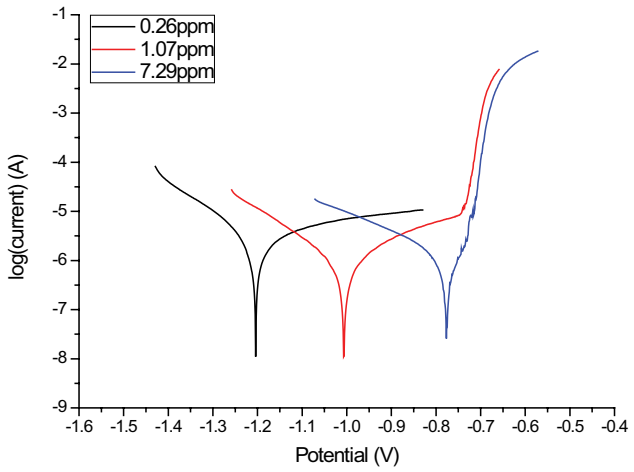

Fig. 6. Polarization curves of 3FL aluminum alloy in seawater with different oxygen concentration.

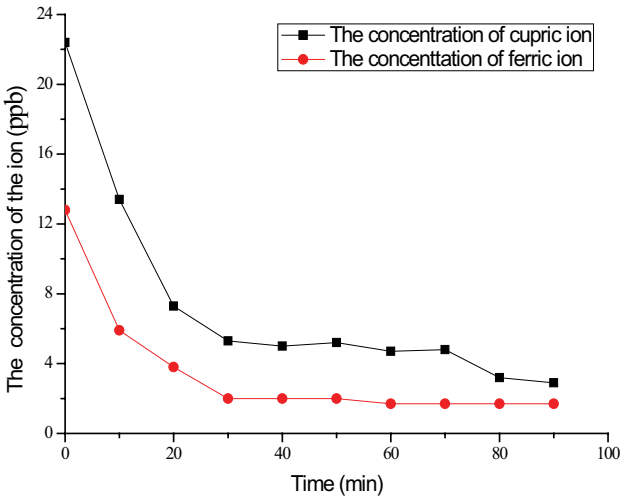

Fig. 7. Concentration change of Cu^{2+} and Fe^{3+} in ion trap.

To investigate the change of Cu^{2+} and Fe^{3+} concentration, the ICP meter is used to measure the concentration. The change of Cu^{2+} and Fe^{3+} concentration with time in the ion trap is shown in Fig. 7 and the change laws of removal percent of Cu^{2+} and Fe^{3+} in the deion process are also shown in Fig. 8. The initial Cu^{2+} concentration is 22.4 ppb, and the Fe^{3+} concentration is 12.7 ppb in natural seawater. The final Cu^{2+} concentration is 2.9 ppb and the Fe^{3+} is 1.7 ppb after 90 min. It is evident that the concentration of Cu^{2+} and Fe^{3+} decreases greatly in the first 30 min, and decreases slowly between 30 and 60 min. The concentration of Fe^{3+} decreases from 0.0127 to 0.0020 mg/L and the removal rate is 84.38% in the first 30 min. For the last 60 min, the removal rate is only 2.8% and ends up with 86.72%. Comparing with Fe^{3+}, the concentration of Cu^{2+} decreases from 0.0224 to 0.0052 mg/L in the first 30 min, and during this time the removal rate is 76.34%. In the last 60 min, the removal rate increases by 10.71% and ends up to 87.05%. Therefore, the pretreatment of the ion trap in the experiment has good deionization performance.

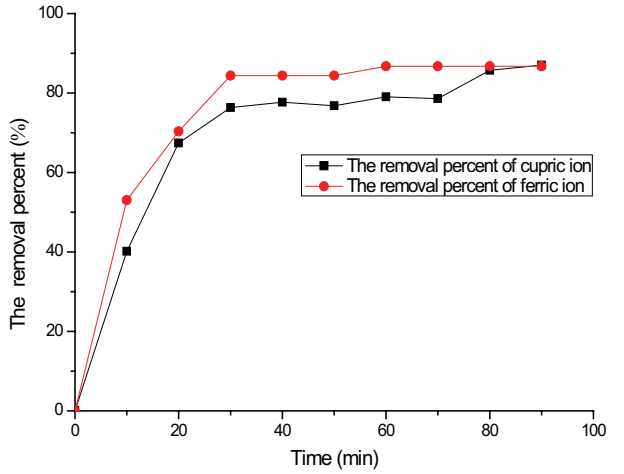

Fig. 8. Change law of removal percent of Cu^{2+} and Fe^{3+} in deion process.

3.2. Effect of deionization on surface corrosion of test tube

3.2.1. Analysis of test tube surface topography

Two different experiments are completed in the evaporator. The difference between the two operational conditions is the concentration of Cu^{2+} and Fe^{3+} in the experiment seawater. The seawater used in the second experiment is deionized by the ion trap, while the other is not. In the experiment process, the surface morphology of the test tube is recorded by a Cannon 5DS camera with 50.6 million pixels.

Fig. 9 shows the development of localized corrosion on the tube surface in the two operational conditions. The surface roughness of the test tubes has increased gradually for 30 h because of the depositing of scaling and the thickening of the passive film ($Al_2O_3 \cdot H_2O$). Scholars [29]

Table 8
Change rule of 3FL aluminum alloy's electrochemical parameters in seawater with different DO concentration

Dissolved oxygen concentration (ppm)	Open circuit potential OCP (V)	Corrosion current density I_{corr} (A)	Corrosion rate C_R (mm/a)
7.29	–0.7709	0.881	0.00928
1.07	–1.0072	0.496	0.00522
0.26	–1.2031	0.404	0.00425

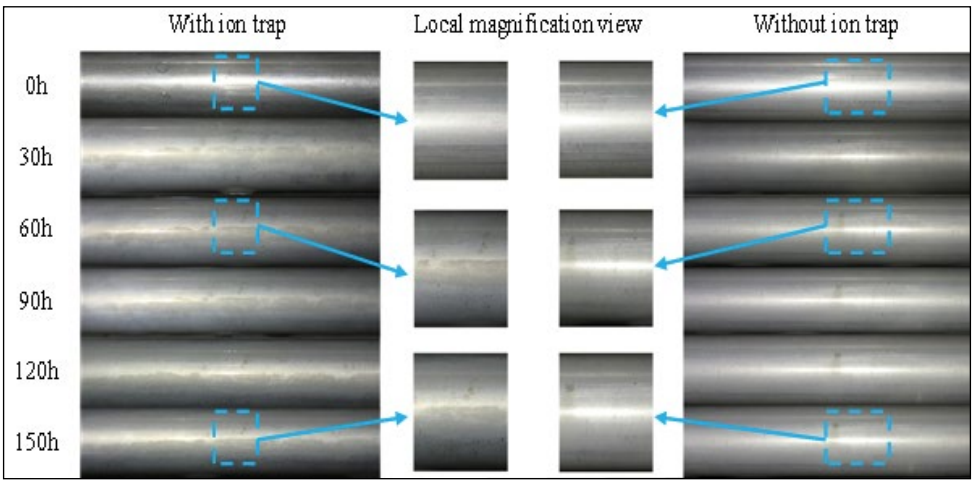

Fig. 9. Development of localized corrosion on the tube surface in two experimental condition.

have indicated that the passive film is only 5–15 nm in the natural condition. The dissolution and generation processes of the passive film occur in water and steam repeatedly. The visual manifestation is that the surface of the test tube gradually loses its luster and presents a milky surface film layer, and the activation of pitting germination often occurs at this stage.

For the experiment with the ion trap, several holes on the tube surface could be found after 60 h. The size changes of these holes are invisible to the naked eye during the entire experiment. Because some particles, such as impurity and pipe scale, damage the tube surface in the erosion process, and then the re-passivation of these localized mechanical damages could inhibit the generation of pitting in this operational condition.

Comparing to the experiment with the ion trap, there are some stable pitting corrosions on the surface of test tubes. Holes generate in 30 h and then grow and deepen between 30 and 120 h. The development of the pits slows down after 120 h. This is because the erosion effect of seawater on corrosion products on the surface of corrosion holes is strengthened after the development of corrosion holes to a certain scale. The corrosion products gradually fall off and cannot maintain the closed environment. The autocatalytic environment of corrosion holes is destroyed and the growth stops. Due to the presence of DO in seawater, the corrosion holes that have stopped growing become passivated again with the participation of oxygen.

The test tube is placed in an ultrasonic bath, washed with nitric acid, soft brushed, and cleaned with pure water after the 150 h of experiment [30]. Keep the photos of the new tube during the installation and compare the test tubes with the new tubes to calculate the pitting number. The morphology of the test tubes after cleaning is shown in Fig. 10, and the number of pitting holes observed under the microscope is listed in Table 9.

Compare the illustrations (1 and 2), (3 and 4) in Fig. 10. The number of pitting holes on the top tube is more than that on the bottom tube. The data in Table 8 attests to the same trend. The reason for this result is that the seawater strikes the top region of the tubes directly. High-speed brine could damage passive film and increase the likelihood of galvanic corrosion. When seawater flows to the bottom region of the tube, its impact force on the surface of test tube decreases due to the presence of gravity and lowered normal velocity. The number of pitting holes on the top is almost twice than that occurs on the bottom in the experiment with the ion trap. This ratio is 1.5 times in the experiment without the ion trap, which means that the washout corrosion is another main corrosion style.

Compare the illustrations (1 and 3), (2 and 4). The number of pitting holes in the experiment without the ion trap is much more than that in the experiment with the ion trap. The significant difference is the direct effect of the presence of the ion trap. As mentioned earlier, the number of Cu^{2+} without the ion trap is 7.7 times than that with the ion trap, and the number of Fe^{3+} without the ion trap is 7.5 times than that with the ion trap. Interestingly, the total number of pitting holes in the experiment without the ion trap is 7.85 times higher in the experiment with the ion trap. The ratio of Cu^{2+} and Fe^{3+} present in seawater is closely related to the ratio of pitting holes. This close relation reveals the influence factors of ions in the corrosion process. In conclusion, the ion trap plays an important role when 3FL tubes are used in the desalination region.

3.2.2. Analysis of surface morphology and corrosion products of test tubes

The images of the test tube's surface are observed by SEM and EDS to analyze the corrosion of the 3FL aluminum alloy tube shown in Fig. 11. The initial conditions of both experiments are the same, except for the pretreatment of seawater. The seawater of the second experiment is deoxidized and deionized, while the other seawater is only deoxidized. Both of the two corrosion experiments are held for 150 h. The test tube is rinsed with pure water and dried in a stoving chest before it is observed by SEM.

Compare the three illustrations (a, b, and f) in Fig. 11. As the images (a and f) show, a white attachment is found on the tube surfaces which are tested in both experiments. To distinguish and analyze the attachment, the surface

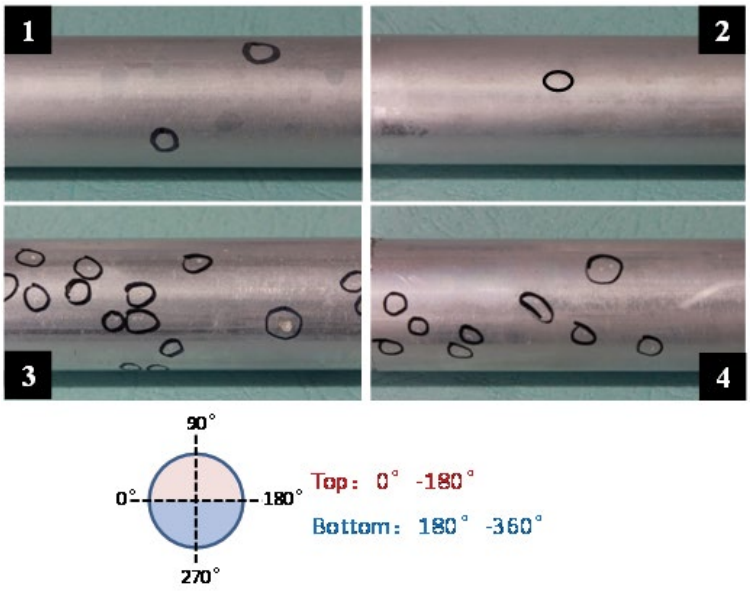

Fig. 10. Pitting morphology of test tubes' surface after removing corrosion product. (1) top morphology of test tube with ion trap, (2) bottom morphology of test tube with ion trap, (3) top morphology of test tube without ion trap, and (4) bottom morphology of test tube without ion trap.

Table 9
Average number of pitting hole on the testing tube surface

Experimental condition	Region	Number of pitting hole/cm^2		Number in Fig. 10
		Diameter > 0.5 mm	Diameter ≤ 0.5 mm	
With ion trap	Top	0	0.033	1
	Bottom	0	0.016	2
Without ion trap	Top	0.0167	0.234	3
	Bottom	0	0.151	4

morphology is magnified 500 times. Image (c) shows that some crystal granules and irregular massive corrosion products are attached to the surface of the tube. The composition of the crystal granules and corrosion product are analyzed by the EDS. The result is given in (d and e), which indicates that the composition of crystal granules is NaCl, while, the composition of corrosion product is $Mg(OH)_2$ and aluminum oxide Al_3O_2 or AlO. The reason why some NaCl is found on the surface is that the NaCl is not washed down during the rinsing. The massive corrosion products observed on the surface are small, and not enough to cover the matrix of aluminum alloy. SEM images of the experiment without ion trap show a small number of corrosion products and much acicular scaling attached to the tube surface (images (f and g)). The acicular scaling and corrosion products are analyzed by EDS. The EDS results indicate that the ratio of $Mg(OH)_2$, $Al(OH)_3$ is lower than that of the experiment with the ion trap. Image (h and i) shows that $CaCO_3$ crystal is the main component of scaling. Since most of the Ca^{2+} had deposited in the ion trap during the deioning process which lasted for 90 min, the weight of deposited $CaCO_3$ is decreased in the deionized seawater. In either of the conditions, there is a small quantity of corrosion product on the test tubes' surfaces, because the cathode reaction is inhibited in the condition of low DO concentration. The corrosion rate goes down with a decrease in DO concentration. Therefore, keeping the DO concentration at a lower level in the seawater desalination process is an effective way to protect the 3FL aluminum alloy.

3.2.3. Analysis of pitting characteristics on the surface of test tubes

Remove the corrosion products from the surface of the test tubes to analyze the pitting of 3FL test tubes. The removing process is according to the national standard (GB/T 16545-2015). The procedure involves dissolving the corrosion product by using HNO_3 [30] and getting the SEM images of the surface of the test tubes. The pitting micromorphology of the test tubes is shown in Fig. 12.

Some mechanical damages and a few oxide particles, which are easy to form pitting corrosion could be found on the surface of an unused 3FL tube shown in SEM image (a) SEM image (b) shows the surface of a 3FL tube used in

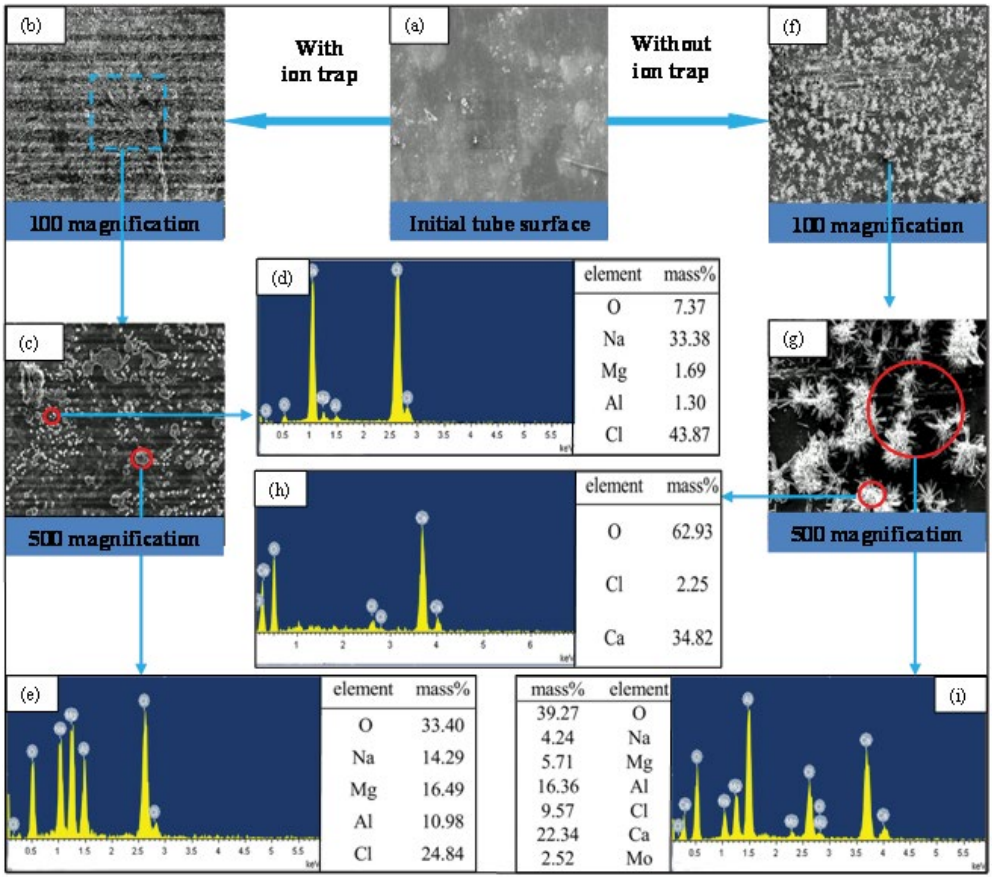

Fig. 11. SEM and EDS images of the two test tube surfaces. (a) The initial tube surface morphology. (b, c, f, and g) The SEM images of the test tube surfaces in two different experiments. (d, e, h, and i) The EDS results of the corrosion product in the two different experiments.

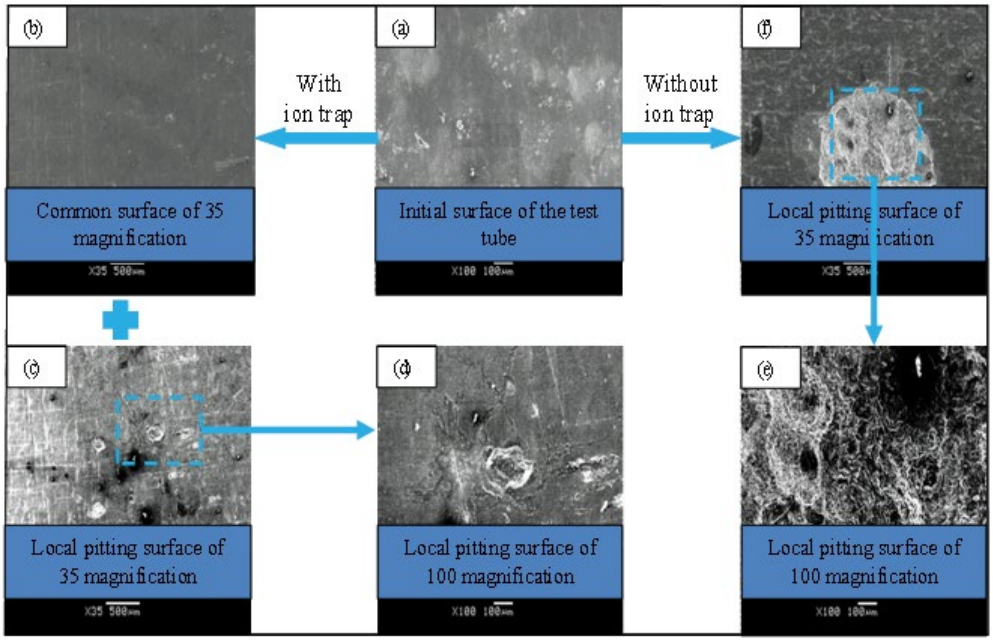

Fig. 12. SEM images of the tubes initial surface and the pits. (a) The initial surface morphology of the test tube. (b)The common morphology of test tube in the second experiment. (c and d) The pitting morphology of test tube in the second experiment. (e and f) The pitting morphology of the test tube in the first experiment.

the experiment with an ion trap, whose characteristics are consistent with the image (a), but few visible pits can be found. A special localized corrosion area is found in the test area which is evident in the image (c), where four visible pits and several micro size pits are located. The diameter of the most significant pit is about 0.1 mm (image (d)). SEM image (f) shows the surface of a 3FL tube tested in the experiment without an ion trap. It can be seen that there are obvious corrosion pits whose depth and pore size are both greater than 1 mm on the surface. Four micro-pittings at the bottom of the corrosion pits can be seen by magnifying 100 times in image (e).

The micro pits tend to generate in the areas of mechanical damages, dislocation, particles of intermetallics, and oxide particles. But, the development of pitting is a complicated process, which is related to many factors, for example, the rate of charge transfer and diffusion control. For the two experiments micro-sized pits are generated, most of which failed to become more prominent. Because the oxidation reaction of aluminum is prolonged in low DO concentration, the corrosion products are not enough to cover the pits. It means that the liquid with a low pH level inside pits could be transferred to outside pits timely. Therefore, the autocatalysis inside pits is inhibited, and the size of the pit remains the same and does not increase. On the other hand, the differences in oxygen concentration between the inside of the pit and the tube surface are quite small, so the oxygen-concentration cell corrosion of the pit area could be neglected.

Some Cu–Al and Fe–Al galvanic couples are generated on the tube surface in the seawater containing heavy metal ions such as Cu^{2+} and Fe^{3+}. The galvanic couples attach to the tube surface and break passive film continuously [31]. A large quantity of oxygen is needed in the restoring process of the passive film so that the development of pits could be observed obviously in the experiment without ion trap within low DO concentration.

Much of the corrosion product is produced by the galvanic couples with the main ingredient on $Al(OH)_3$ in the corrosion reaction. The corrosion product will cover the pits and inhibit the diffusion of the solution inside of pits. With the dissolution of the aluminum in pits, the concentration of aluminum ion increases continuously. As a result, it causes the Cl^- to move from seawater to the solution sealed in pits. The hydrolysis reaction of $AlCl_3$ generates high quantities of H^+; therefore, the pH of the pitting solution is decreased in this period. The corrosion rate of aluminum will be accelerated in this acidic condition. Then the pits will expand rapidly. In both of the experiments, seawater is sprayed from the distribution tube and wash the corrosion product attached to the tube surface constantly. With the expansion of the pits and the washing of flowing seawater, the corrosion product generates and falls off continuously. When the covering of pits is destroyed, the seawater will mix with the solution sealed in pits. The pitting corrosion will be inhibited because of the re-passivation of pits. This re-passivation is the reason why the pit stops growing in the experiment without the ion trap after 120 h. By comparing the results of the two tests, the Cu^{2+} and Fe^{3+} have great effects on the pitting corrosion of the 3FL aluminum alloy. While the concentrations of Cu^{2+} and Fe^{3+} are kept below 3 ppb with the ion trap, the diameter and depth of pits decrease significantly. Therefore, the pretreatment whose function is to remove Cu^{2+} and Fe^{3+} from seawater is necessary before the seawater flows into the evaporator.

3.2.4. Analysis of electrochemical experiment results

The relationship between the polarization curve of 3FL aluminum alloy and the time of seawater deionization is studied by the electrochemical experiment, as shown in Fig. 13. The stable OCP of the working electrode in the seawater solution is measured by an electrochemical workstation, as shown in Fig. 14. Corrosion current density (I_{corr}) of the working electrode in different seawater can be obtained by the Tafel curve extrapolation method. The average corrosion rate (C_R) of the working electrode can be obtained from the measured average corrosion current density, as in Eq. (5) [28]. All results are shown in Table 10.

In the five sets of experiments, the basic trends of the polarization curves are the same, as shown in Fig. 13. The current on the surface of the working electrode from –0.735 to –0.625 V rapidly increases to 10 mA, and the working electrode has pitting corrosion in this voltage range. The OCP can characterize the corrosion sensitivity of the material in solution. It can be found in Fig. 14 that the OCP of the 3FL aluminum alloy material in seawater is relatively positive, which indicates that the material has good passivation performance in the seawater solution. The extension of the deionization time does not cause a significant change in the OCP. The variation of the OCP in the five groups of experiments is only 0.05 V. Therefore, the tendency of material corrosion does not change significantly after the deionization treatment.

As shown in Fig. 15, the I_{corr} gradually decreases as the deionization time increases. In the seawater after 10 min

Table 10
Change law of 3FL aluminum alloy's electrochemical parameters in seawater with different deion time

Deionized time (min)	Open circuit potential OCP (V)	Corrosion current density I_{corr} (A)	Corrosion rate C_R (mm/a)
0	–0.7633	1.223	0.0129
10	–0.7944	1.069	0.0113
20	–0.7652	0.952	0.0100
50	–0.7765	0.9	0.0095
90	–0.7709	0.881	0.0093

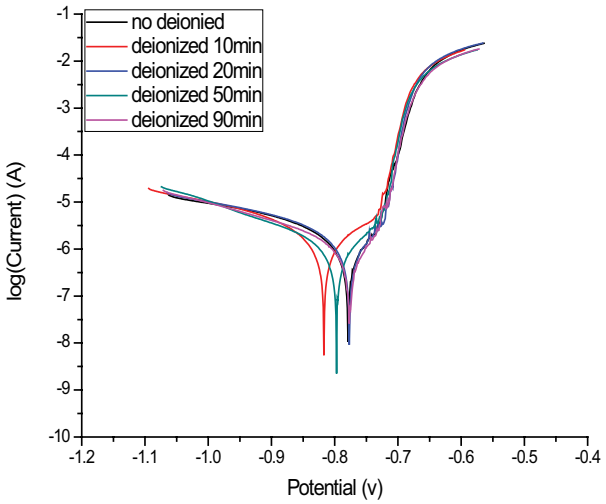

Fig. 13. Polarization curves of 3FL aluminum alloy in seawater with different deion time.

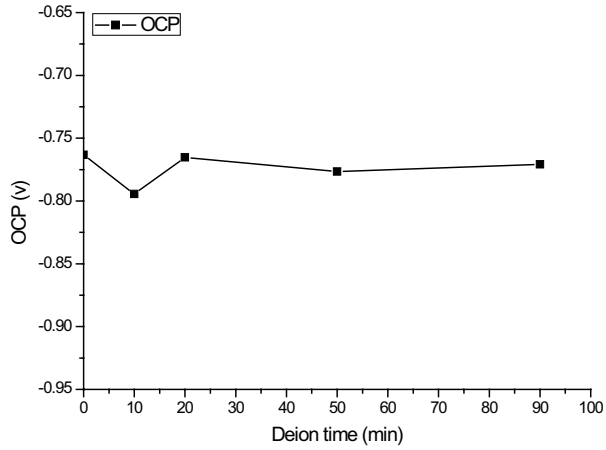

Fig. 14. Change rule of OCP with deion time.

of deionization, I_{corr} decreased rapidly, which is 12.6% lower than the original seawater I_{corr}. After 20 min, the I_{corr} is 22.16% lower than the original seawater. After 50 and 90 min of deionization, I_{corr} decreases by 26.41% and 27.9%. The corrosion rate has the same regularity. Therefore, after the deionization treatment, the corrosion rate of the aluminum alloy sample is remarkably lowered, and the effect of the pre-deionization period is more remarkable. As the deionization progresses, the rate of decline of I_{corr} is also gradually slowed down, which is consistent with the variation of the concentrations of Cu^{2+} and Fe^{3+}. Mainly because heavy metal ions in seawater are removed after deionization treatment, the concentration of heavy metal ions is gradually reduced. The number of corrosion couple pairs formed on the surface of aluminum alloy samples is constantly reduced, the corrosion rate is continuously reduced. At the beginning of the deionization process, the concentration of Cu^{2+} and Fe^{3+} is higher, so the reaction speed is faster. As the reaction proceeds, the concentration of the reactants

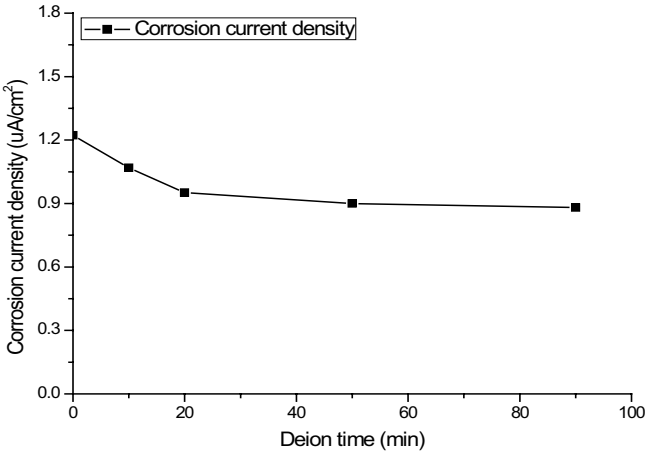

Fig. 15. Change law of corrosion current density with deion time.

gradually decreases, and the reaction rate also decreases, and then the corrosion rate tends to decrease.

3.3. Effect of seawater erosion on the surface of test tubes

The effect of seawater scour on the corrosion of the test tube is studied by adding a dummy tube to change the tube pitch. The outer diameter of the supply tube is 45 mm, the outer diameter of the test tube and the dummy tube is 25.4 mm, shown in Fig. 16. In the second operational condition with the dummy tube, the center distance between the test tubes is 57.2 mm. In the third operational condition (without dummy tube), the center distance between the supply tube and the test tube is 107.2 mm. The material of the dummy tube and the test tube are both 3FL aluminum alloy. The seawater is treated by deionization to reduce the concentration of Cu^{2+} and Fe^{3+} in the seawater to below 5 ppb before the start of the corrosion experiment.

3.3.1. Analysis of surface topography of test tubes

Choosing 30 h to display and contrast the surface topography. In Fig. 17, the picture on the left shows the operational condition without the dummy tube and the right picture shows the operational one with the dummy tube.

In the operational condition without the dummy tube, it can be found from the 30th hour that the surface of the test tube is covered with a layer of white deposits which are mainly corrosion products of Al and Mg found by the EDS. The accumulation of corrosion products increases with the extension of the experimental time. When the experiment is carried out for 150 h, the corrosion product layer with uneven distribution on the surface of the test tube can be observed. The uneven deposition of the surface corrosion products causes a significant change in the surface roughness of the test tube. In the operational condition with the dummy tube, it can be seen the surface of test tubes lose luster during 30 h as well. On the one hand, the surface roughness of test tubes are changed by the deposition in the experimental seawater. On the other hand, the dense oxide film on the surface of the test tube caused structural damage due to the erosion of seawater and the oxidation of the surface.

Observing the surface of the test tube under the operational condition without the dummy tube, the black damage area appeared on the top surface. The damaged area is mainly formed by the combination of dirt and corrosion caused by tiny flaws on the surface of the test tubes. The bottom surface is light gray and smooth, and the oxide film is evenly covered on the surface of the test tubes. There is no impact corrosion phenomenon, mainly because the top surface of the test tube is around the 0° impact zone, and the liquid film fluctuates sharply. On the one hand, the shearing force of seawater on the oxide film, corrosion product layers, and aluminum alloy matrix are strengthened. On the other hand, the increase in the fluctuation of the liquid film will cause the supply rate of oxygen to increase and the corrosion rate will increase in the corrosion reaction. Observing the test tubes under the operational condition with the dummy tube, there is no obvious erosion-corrosion mark and pitting corrosion on the surface of the top and the bottom, which maintains a good finish.

Therefore, comparing the top surface morphology of the two test tubes, it can be found that the degree of erosion-corrosion of the top surface is significantly reduced after adding the dummy tube. There must be a critical tube pitch in the erosion-corrosion of aluminum alloy test tubes in horizontal tubes falling film evaporators. When the tube pitch is greater than the critical value, the damage caused by erosion-corrosion is significantly accelerated. When the tube pitch is less than the critical value, the erosion-corrosion is relatively slow, which has the same principle as the critical flow rate obtained by Yue-yi [12] experimental study.

3.3.2. Analysis of surface morphology and corrosion products of test tubes

The SEM corrosion morphology of the test tube surface magnified 100, 200, 500, and 1,000 times in the condition without the dummy tube is shown in Figs. 18(1–4). Analysis of the 100-fold SEM image (1) reveals that the surface of the test tube is covered with a large number of scaly attachments that densely cover most of the sample area. The erosion of seawater causes an increase in the corrosion rate and corrosion products. In the meantime, the shear force of the

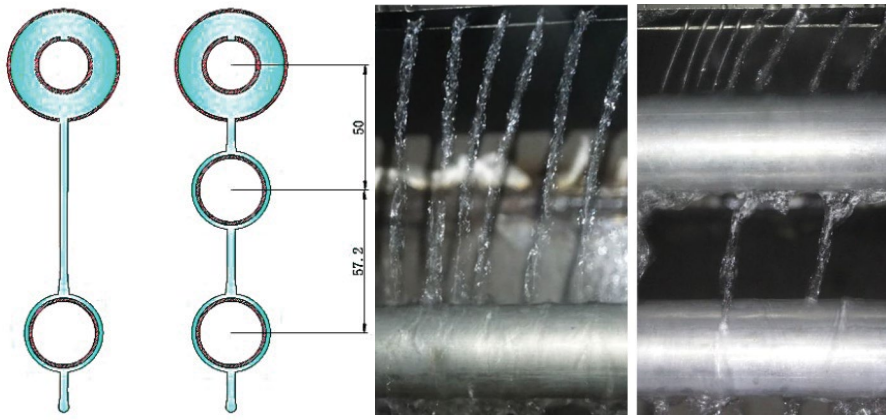

Fig. 16. Schematic diagram of the change of tube pitch in experiments.

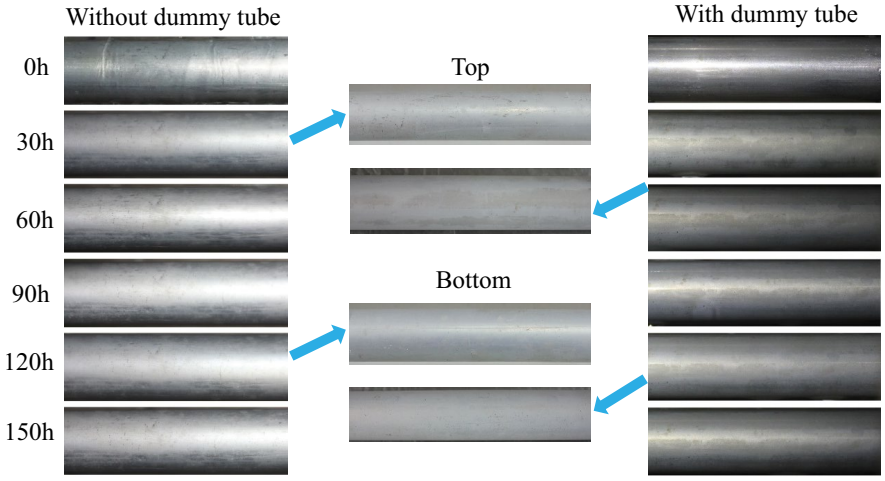

Fig. 17. Change rules of test tubes' morphology in both experiments with time goes by.

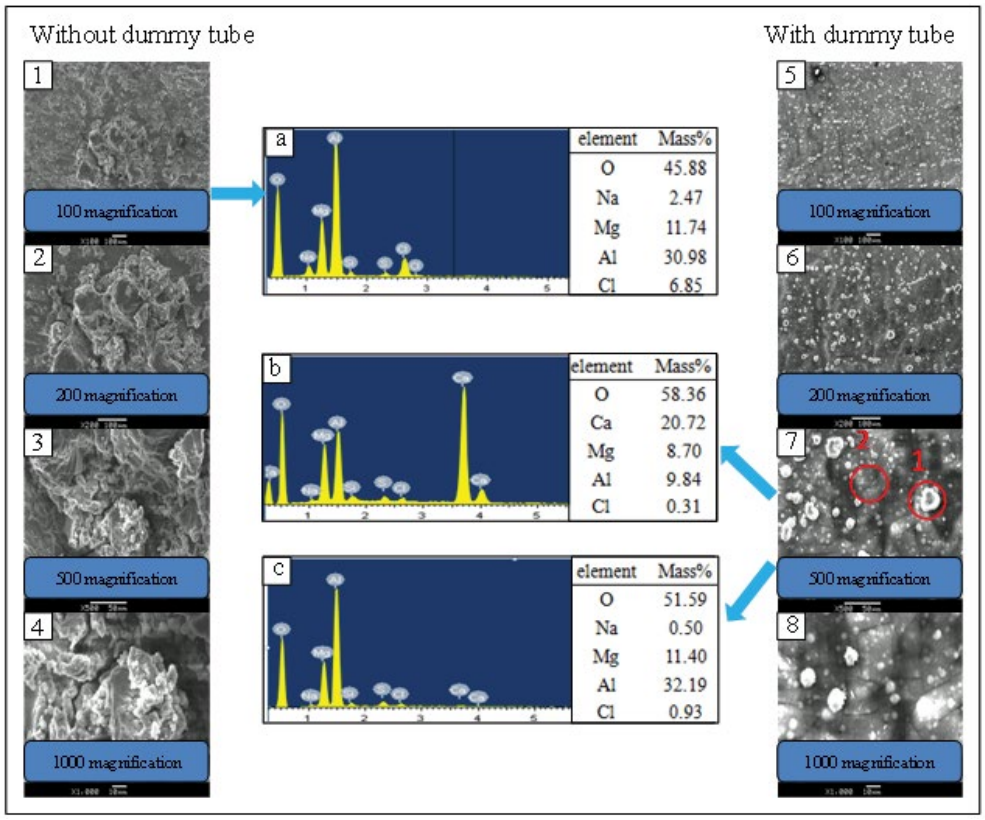

Fig. 18. SEM and EDS images of the two test tubes surfaces. (1–4) The SEM images of the test tubes surface in the condition without dummy tube. (5–8) The SEM images of the test tubes surface in the condition with dummy tube. (a–c) The EDS results of the corrosion product in the two different experiments.

seawater wash on the corrosion product peels off a certain quantity of corrosion products. Under the joint action, the surface features of the surface corrosion products of the test tube are unevenly distributed in scale. In addition, there is relatively obvious sediment with a diameter of about 200 μm in the center of the picture. Amplification of the sediments at different multiples reveals that the shape of the protrusions is an irregular column and the bottom is a large block of corrosion products, as shown in (2 and 3). The protrusions on the surface may be formed by the accumulation of corrosion products around the holes. The sample whose surface unevenly deposited with cluster-like scale deposits is enlarged as shown in (4).

The test result of the elemental composition of the corrosion products and scale which are measured by an X-ray energy spectrometer is shown in Fig. 18a. It shows that the most important element in the attachment on the surface of the sample is oxygen, accounting for 45.88%. The cluster-like scale conforms to the characteristic form of $Mg(OH)_2$, and a large amount of Mg also present in the energy spectrum result, so the main component of the scale attached to the corrosion product is $Mg(OH)_2$. The source of $Mg(OH)_2$ has two routes. On one hand, the combination of Mg^{2+} and OH^- in the original seawater is deposited. On the other hand, the metal Mg and its oxide on the surface of the aluminum alloy are corroded in seawater and form the corrosion product of $Mg(OH)_2$ adhered to the surface of tubes.

In the operational condition with the dummy tube, the surface topography of the test tube surface magnified 100, 200, 500, and 1,000 times are shown in Figs. 18(5–8). By observing a 100-fold SEM image, it is found that the surface of the sample is distributed with dot-like deposits, which are scattered on the surface of the tube and could not form a uniform coverage on the surface of the tube. When the magnification is 500 times, it can be found that the shape of these attachments is not uniform, and there are some cluster-like uniformly distributed attachments under the needle-like attachments, as shown in Fig. 18(7). When magnified to 1,000 times, it can be found that the shape of the circular attachments is a cluster of needles, which is presumed to be the $CaCO_3$ scale. There is a layer of cluster-like substance covered by $CaCO_3$. It is speculated that $CaCO_3$ is attached to $Mg(OH)_2$ for growth.

The composition of the different attachments on the surface of the sample is analyzed by EDS, as shown by the red wireframe 1and 2 in Fig. 18(7). Firstly, a cluster of needle-like substances in red wire frame1 is analyzed. The analysis results show that the main elements are oxygen and calcium, and a small quantity of Mg and Al, as shown in Fig. 18b. Therefore, it can be inferred that the circular needle clusters scattered on the sample surface are $CaCO_3$ scales. The energy spectrum analysis of red wireframe 2 revealed that the main elements are oxygen, aluminum, and magnesium. It is inferred from mass percentage and

atomic percentage calculation that there are $Mg(OH)_2$ and corrosion products of aluminum in the test area. Because the accumulation of corrosion products on the sample surface is not obvious and the structure is dense, it is speculated that the corrosion products may exist in the form of $[AlO(OH)]_2$.

Comparing the surface morphology of the test tubes in the two sets of operational conditions, it can be found that $CaCO_3$ is attached to $Mg(OH)_2$ scales for growth on the surface of the test tubes. The amount of $CaCO_3$ deposited on the surface of the test tube without the dummy tube is relatively small. This is mainly because $CaCO_3$ is a slag-like scale and the adsorption force on the surface of the tube is not strong. As the tube pitch increases, the impact of seawater on the test tube is enhanced, causing a portion of $CaCO_3$ to detach from the surface of the test tube. In the two experiments, the number of corrosion products on the surface of the test tube and the existing forms are significantly different. As the tube pitch decreases, the quantity of corrosion products on the surface of the test tube is significantly reduced, and the form of the corrosion product changes from a scaly dense distribution to a dense film layer.

3.3.3. Analysis of pitting characteristics on the surface of test tubes

According to the national standard, after removing the corrosion products on the surface of the test tube by concentrated nitric acid, the diameter, density, and morphology of pitting on the surface of the test tube are analyzed, as shown in Fig. 19. Table 11 lists the pitting of the top and bottom of the test tubes under two conditions.

Under the third operational condition (without dummy tube), the pitting corrosion distribution on the top and bottom of the test tube are shown in Figs. 19a and d, respectively, and the number of pitting is small. The diameters are all less than 0.5 mm. According to statistical calculation, the pitting density of the top surface is 0.051/cm^2, and the pitting density of the bottom surface is 0.033/cm^2. Under the second operational condition (with dummy tube), the pitting corrosion distribution of the top and bottom surfaces of the test tubes are shown in Figs. 19b and c. The surface of the test tube has a weak pitting degree and the diameter is less than 0.5 mm. The pitting density is 0.016/cm^2 and the bottom pitting density is 0.032/cm^2.

Select the pitting area on the surface of the test tubes for slicing and prepare test samples for SEM, as shown in Fig. 19. Figs. 19(1 and 2) are the appearance of the etched holes magnified 100 and 500 times in the condition without the dummy tube.

The analysis shows that the etched holes appear as inverted cones, with the diameter of 100–200 mm and greater than 100 mm in depth. The inside of the etched holes is a granular rough surface. The corrosion condition of the inner wall of the etched hole indicates that the metal in the etched hole is always in the activated state. The aluminum alloy matrix is continuously dissolved, and the etched hole still has the potential for deep digging at the end of the experiment. This is mainly because the pitting core here is covered by the corrosion products, and the Cl^- is continuously moved into the pores through the porous corrosion product layer to form $AlCl_3$. The $AlCl_3$ is continuously hydrolyzed to produce H^+, and the autocatalyst is continuously carried out. The pH of the solution in the etched hole is continuously lowered, and the etched holes are continuously deepened.

In the operational condition with the dummy tube, after removing the corrosion products on the surface of the test tube, the surface morphology of the sample is analyzed 100

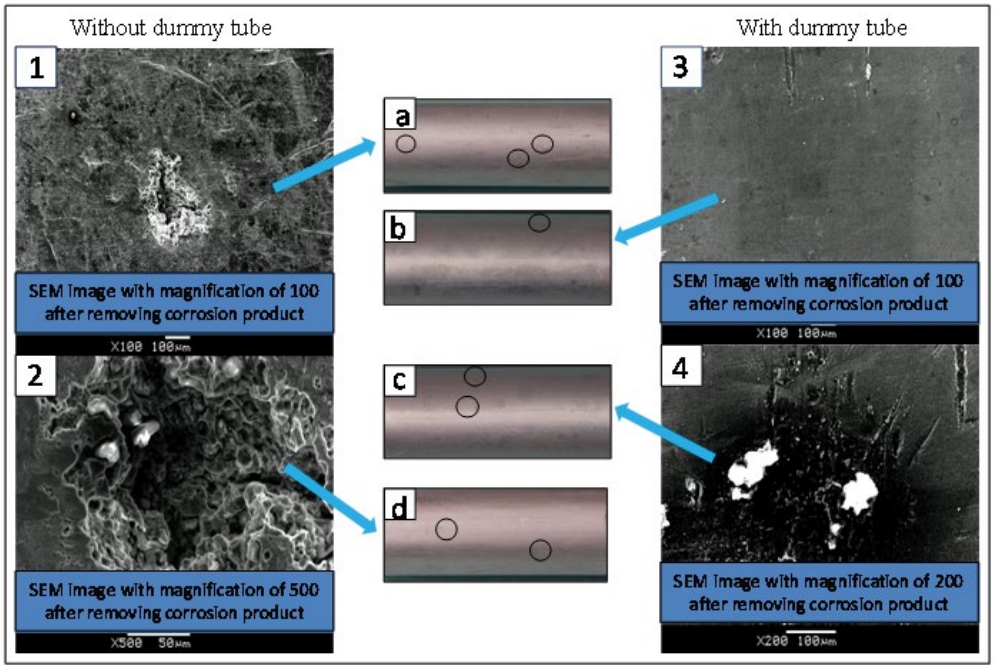

Fig. 19. Pitting micro morphology of test tube in the condition (1 and 2) (a and d) without dummy tube and (3 and 4) (b and c) with dummy tube.

Table 11
Average number of pitting hole on the testing tube surface

Experimental condition	Region	Number of pitting hole/cm^2	Number in Fig. 18
With dummy tube	Top	0.016	b
	Bottom	0.032	c
Without dummy tube	Top	0.051	a
	Bottom	0.033	d

and 200 times, as shown in Fig. 19(3 and 4). It can be seen that most detection areas maintain a good surface topography, and no obvious etch holes exist. There are two flaw areas on the surface, and the oxide does not fall off after pickling. The diameters of the flaw areas are about 0.1 mm, which may form the germination of pitting.

Comparing the pitting corrosion on the surface of the two test tubes, it can be found that the pitting corrosion of the test tube surface is not severe in the two experiments. Pitting on the growing period is found on the surface of the test tube in the operational condition without the dummy tube. The germination of pitting is found on the surface of the test tube in the operational condition with the dummy tube. The seawater scour accelerates the corrosion reaction process, and the average corrosion rate is accelerated, which is intuitively reflected in the increase in the number of corrosion products. The increase in the number of corrosion products tends to cause a part of the pitting germination to be covered under the corrosion products, which provides favorable conditions for the development of pitting germination to stable pitting. Comparing the pitting density and diameter of the surface of the two test tubes, it can be found that seawater scour can accelerate the formation and development of pitting corrosion, the pitting corrosion diameter, and pitting density increase.

4. Conclusion

This paper investigates the feasibility of applying a 3FL aluminum alloy tube in the LT-MED desalination plant. The electrochemical corrosion experimental platform and a horizontal tube falling film corrosion experimental platform are set up. It compares the deoxidation and deoxygenation deionization conditions of aluminum alloy tubes whose surface corrosion morphology and pitting corrosion characteristics and studies corrosion law of seawater corrosion on aluminum alloy tube. This provides a reference for the application of 3FL aluminum alloy tubes in LT-MED desalination plants and provides suggestions for anticorrosion. Conclusions are summarized as follows:

- Most of the Cu^{2+} and Fe^{3+} dissolved in the seawater are removed in the first 30 min in this experiment. The highest removal rate of Fe^{3+} is 86.72% in this ion trap. Meanwhile, the removal rate for Cu^{2+} is 87.05%.
- With the extension of the deionization time, the OCP of the material does not change significantly and the corrosion rate gradually decreases. In seawater with 90 min of deionization, the corrosion rate of the sample is reduced by 21.6% compared to the initial seawater. When the oxygen concentration in seawater decreases from 7.29 to 0.26 ppm, the corrosion rate of the sample decreases by 54.5%.
- The heavy metal ions can promote the growth of micropits into stable pits located on 3FL aluminum alloy tubes in the evaporator. The re-passivation of pits can inhibit the development of pits conspicuously.
- The Cu^{2+} and Fe^{3+} have a significant effect on 3FL aluminum alloy's pitting corrosion, even at low concentrations. The diameter of the pits observed is over 1 mm when the seawater is not pretreated in the ion trap. However, the diameter of pits is about 0.1 mm when the seawater is pretreated in the ion trap where the concentration of Cu^{2+} and Fe^{3+} decreases to 3 ppb.
- The erosion of seawater causes significant damages to the surface of the aluminum alloy. When the dummy tube is not added (the tube pitch is 107.2 mm), the corrosion products on the surface of the test tube are mainly densely distributed in a scaly structure. When the dummy tube is added (the tube pitch is reduced to 57.2 mm), the corrosion product on the surface of the test tube is dense and the quantity of corrosion products is also significantly reduced.
- Seawater scouring will accelerate the corrosion rate and increase the amount of corrosion products. At the same time, the shearing force of the seawater scour on the corrosion products will peel off a certain amount of corrosion products. Under the combined effect of these two, the test tube surface corrosion products will show irregular scale-like distribution, and the increase in the amount of corrosion products caused by seawater scour will cause some pitting germination to be covered, which provides favorable conditions for the development of pitting germination to stable pitting.
- In the design of the evaporator, the deoxidation process and the ion trap must be considered, and it must be ensured that the design of the tube bundles reduces the tube pitch. It is recommended to use a rotated triangular tube layout or quadrilateral tube arrangement.

Acknowledgment

The research is supported by the Project of National Science Foundation of China (No. 51406024) and the

Fundamental Research Funds for the Central Universities (No. DUT19LAB19).

Symbols

I_{corr} — Corrosion current density, mA/m^2
M — The relative atomic weight of the metal
ρ — Density, g/cm^3
C_R — Corrosion rate, mm/a
σ_x — Standard deviation of direct measurements
σ_y — Standard deviation of undirect measurements

References

[1] L. Erjing, The thermal seawater desalination technology and its application, Power Equip., 23 (2009) 147–150.
[2] Y. Kailu, L. Qingchun, X. Feng, R. Guoling, Preliminary study on the application of modified aluminum alloy in thermal desalination apparatus, Ship Sci. Technol., 30 (2008) 213–217.
[3] W. Guo-jun, L. Xin-yu, The chemical composition and phase composition of aluminum alloy 7055 and its performance characteristics, Shanghai Nonferrous Met., 29 (2008) 118–122.
[4] X. Guangyao, Process investigation on aluminium alloy cutting with HS-WEDM, Electromachining Mould, 6 (2002) 43–45.
[5] W. Xiongfei, P. Hongxia, The milling force and process of thin-web aluminum alloy parts in high-speed cutting, Group Technol. Prod. Mod., 26 (2009) 53–56.
[6] Z. Xinming, D. Yunlai, Z. Yong, Development of high strength aluminum alloys and processing techniques for the materials, Acta Metall. Sin., 51 (2015) 257–271.
[7] Y. Xianfang, L. Tianquan, W. Wei, Z. Cuihua, Progress of environment-friendly chemical surface treatment of aluminum alloys, Mater. Rev., 28 (2014) 439–442.
[8] X. Lixin, X. Chengxiang,W. Shichang, Corrosion behavior of aluminum alloy in seawater, Chem. Ind. Eng., 32 (2013) 47–51.
[9] Z. Ahmed, Corrosion and corrosion prevention of aluminium alloys in desalination plants: part 2, Anti-Corros. Methods Mater., 28 (1981) 4–10.
[10] P. Wencai, H. Jian, G. Weimin, K. Yafei, Effect of temperature and dissolved oxygen on corrosion performance of alloy 5083 in seawater, Equip. Environ. Eng., 7 (2009) 22–26.
[11] G. Hongda, Research on Corrosion Behaviors of Aluminium Tubes in Horizontal Tube Falling Film Evaporator, Dalian University of Technology, 2014.
[12] W. Yue-yi, Corrosion behavior of aluminum alloy in flowing seawater, Equip. Environ. Eng., 2 (2005) 72–76.
[13] S. Lin, Corrosion Behavior and Impressed Current Cathodic Protection of Aluminum Alloy in 3.5% Sodioum Chloride Solution, Harbin Engineering University, 2012.
[14] R.E. Melchers, Influence of temperature on sea water immersion corrosion of aluminium (UNS A95086), Br. Corros. J., 36 (2001) 201–204.
[15] T. Jiqiang, The Electrochemical Corrosion Behavior of Tungsten Aluminum (W-Al) Alloy in Nacl Solution, Ocean University of China, 2013.
[16] N. Birbilis,R.G. Buchheit, Investigation and discussion of characteristics for intermetallic phases common to aluminum alloys as a function of solution pH, J. Electrochem. Soc., 155 (2008) C117–C126.
[17] B. Zaid, D. Saidi, A. Benzaid, S. Hadji, Effects of pH and chloride concentration on pitting corrosion of AA6061 aluminum alloy, Corros. Sci., 50 (2008) 1841–1847.
[18] F. Sato,Y. Asakawa, Localized corrosion behavior of aluminum-magnesium-silicon alloy in ground water, Corros. J. Sci. Eng., 55 (1999) 522–529.
[19] W. Kunyu. The Effect of Ion Trap Pretreatment Process on Corrosion of Aluminum Alloy Tube, Dalian University of Technology, 2013.
[20] H. Yu-zhou, D. Li-hua, L. Bo-yang, Current status and development trend of study on corrosion of aluminum alloy in deep sea, Mater. Prot., 47 (2014) 44–47, 49, 54.
[21] T. Zhiguo, Study on Removal of Heavy Metal Ions in Seawater by Redox, Tianjin University, 2012.
[22] O.K. Abiola, J.O.E. Otaigbe, Effect of common water contaminants on the corrosion of aluminium alloys in ethylene glycol–water solution, Corros. Sci., 50 (2008) 242–247.
[23] W. Hongren, W. Jianhua, W. Juntao, W. Hongbin, F. Zhigang, Study on the corrosion & electrochemical properties of alloy AA5083 and the effect of active chlorine in seawater, Electrochemistry, 9 (2003) 60–65.
[24] Z. Liu, J. Wang, P. Zhang, Y. Wang, Y. Zhang, Corrosion behavior of 5083 Al-alloy in seawater and its cathodic protection, J. Chin. Soc. Corros. Prot., 35 (2015) 239–244.
[25] L. Bazzi, R. Salghi, Z. El Alami, E. Ait Addi, S. El Issami, S. Kertit, B. Hammouti, Comparative study of corrosion resistance for 6063 and 3003 aluminium alloys in chloride medium, Rev. Métall., 100 (2003) 1227–1235.
[26] P. Changjun, C. Gusheng, A demonstration of Raoult's law and Herry's law by using adsorption theory, J. Wuhan Inst. Technol., 17 (1995) 20–22.
[27] Q. Qinggang, Y. Yue, M. Xingsen, S. Shengqiang, Experimental Study on Fouling and Corrosion Characteristics of 3FL Aluminum Alloy Heat Exchange Tubes in Deoxidized Fresh Seawater, The Twenty-first National Academic Conference of the Engineering Thermophysics Committee of the Institute of Higher Education, Yangzhou, Jiangsu Province, China, 2015, pp. 226–233.
[28] Z. Wenmeng, Study on Aluminum Alloy Heat-Transfer Tube in Horizontal Tube Falling Film Evaporation Desalination, Tianjin university, 2014.
[29] H. Zhe, Technical and Performance Study of Chromate-Free Chemical Oxide Film on Aluminum Alloy, Beijing University of Chemical Technology, 2008.
[30] GT 16545–2015/ISO8407, Corrosion of Metals and Alloy-Removal of Corrosion Products from Corrosion Test Specimens, 2009.
[31] I. Bakos, S. Skabó, Corrosion behaviour of aluminum in copper containing environment, Corros. Sci., 50 (2008) 200–205.